A Fluidically Tunable, Dual-Band Patch Antenna With Closely Spaced Bands of Operation

Tonmoy Bhattacharjee, *Student Member, IEEE*, Hongrui Jiang, *Senior Member, IEEE*, and Nader Behdad, *Senior Member, IEEE*

***Abstract*—We present a new technique for designing a dual-band patch antenna with closely spaced bands of operation, whose response can be changed dynamically using a fluidic tuning mechanism. Using this technique, a dual-band tunable patch antenna operating at around 2.5 GHz is designed and fabricated using 3-D printing. Two oil-filled channels are placed in the substrate of the antenna along the nonradiating edges of the patch and filled with movable metal cylinders. As the cylinders are introduced underneath the patch, it starts to exhibit a dual resonant behavior with both resonances having a similar electric current distribution. The separation between the two resonant frequencies is a function of the relative position of the metallic cylinders underneath the patch antenna. As the overlap volume between the metal cylinders and the patch increases, the frequency of the first band, f_1, starts to decrease and that of the second band, f_2, increases. The maximum separation between f_1 and f_2 is achieved when half of the lengths of the metallic cylinders are underneath the patch. The prototype device designed in this work can achieve frequency ratios in the range of $f_2/f_1 = 1.08$–1.30. The antenna demonstrates similar radiation characteristics at both bands of operation.**

***Index Terms*—3-D printing, dual-band antennas, patch antennas, reconfigurable antennas.**

I. Introduction

With the recent developments in wireless communication and voracious appetite for data, there is a growing trend toward using wireless devices that operate at two or more frequency bands. The frequency bands used for a given wireless application (e.g., cellular communication) generally vary based on the geographical location and the service provider. This has been a motivating factor for developing antennas that can work at multiple bands simultaneously and dynamically change their operating bands that they work at if needed. Reconfigurable antennas in the past decade or so have gained a remarkable research interest. They are used to support multiple telecommunications standards, to mitigate strong interference signals, or to cope with a changing environment [1]. Using reconfigurable antennas can also enable the efficient use of power and spectrum, reduce the number of complex hardware, and potentially reduce the cost of the system.

Manuscript received March 26, 2015; revised April 23, 2015; accepted May 10, 2015. Date of publication May 12, 2015; date of current version February 08, 2016. This material is based upon work supported by the U.S. National Science Foundation under Award No. ECCS-1101146.

The authors are with the Department of Electrical and Computer Engineering, University of Wisconsin–Madison, Madison, WI 53706 USA (e-mail: tbhattacharj@wisc.edu; hongrui@engr.wisc.edu; behdad@wisc.edu).

Color versions of one or more of the figures in this letter are available online at http://ieeexplore.ieee.org.

Digital Object Identifier 10.1109/LAWP.2015.2432575

Reconfigurable antennas may be designed to provide tunable frequency bands, dynamically alter their polarizations, or have variable radiation patterns. Various techniques have been used to achieve agility in frequency, polarization, and beam direction of antennas. Among these, using radio-frequency microelectromechanical systems (RF-MEMS), variable capacitors (varactors), PIN diodes, photoconductive elements, physical alteration of the radiating structure, and advanced materials such as ferrites and liquid crystals can be mentioned [1]–[3]. For example, in [4], PIN diode switchable slots are used in a microstrip patch antenna to achieve circular polarization diversity. In [5], a rectangular spiral antenna is loaded with a set of MEMS switches to provide scan-beam capability, and in [6] a varactor-tunable, dual-band slot antenna is presented. While there are many more examples of reconfigurable antennas available in the literature, these examples sufficiently illustrate the variety of different electronic techniques used to reconfigure the various properties of antennas. Electronically tunable antennas, however, suffer from nonlinearities under moderate to high peak-power excitation levels. These nonlinearities can result in intermodulation distortion and RF-induced changes of the antenna's radiation parameters. This limits the use of these tuning techniques mainly to the receiving systems or low-power transceivers.

In this letter, we present a new concept for designing dual-band patch antennas with closely spaced bands of operation and similar radiation characteristics at both bands. This technique can be used to design dual-band antennas with frequency ratios as low as $f_2/f_1 = 1.08$. We also present a fluidic technique that can be used to dynamically tune the frequency responses of the proposed antenna. The fluidic tuning technique used in this work is similar to those used to design tunable periodic structures in [7] and [8]. In [7], these techniques were demonstrated to be far superior to electronic tuning technique in terms of the linearity of the response of the structure when subjected to moderately high-power levels (tens of watts). A prototype of this dual-band tunable antenna is designed and fabricated and experimentally characterized in the lab. The results presented in this letter are significant for two reasons. First, designing dual-band antennas with small band separation, and similar radiation characteristics at both bands, is a rather challenging task. Therefore, the concept presented in this work (even in its static form) is expected to find applications in practical systems that need to operate under such conditions. Second, the proposed mechanical tuning technique is ideally suited for transceiver systems that need to work with moderate to high peak-power levels. This is an area where most conventional electronic tuning techniques drastically underperform.

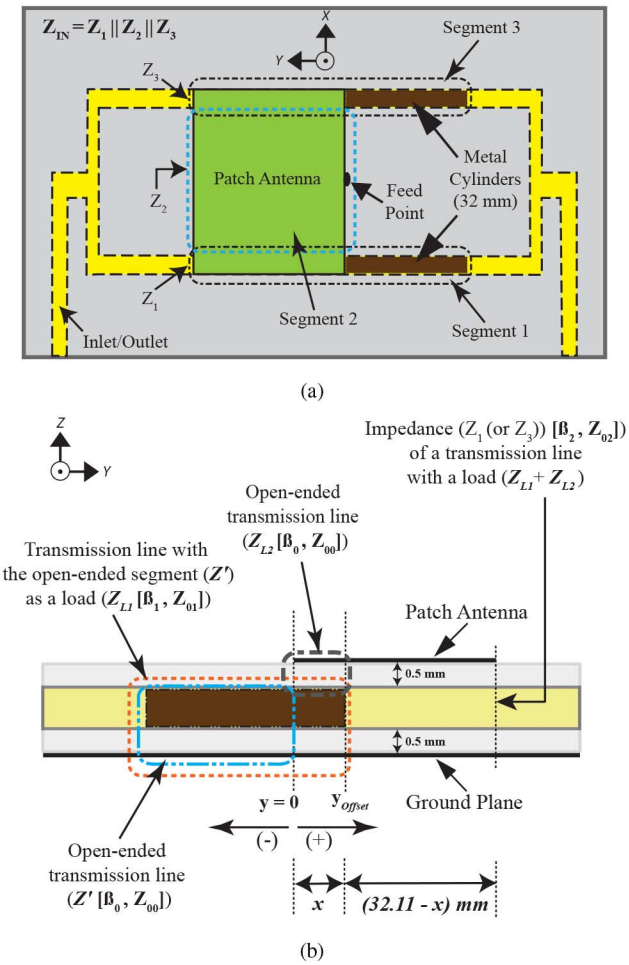

Fig. 1. Layout of the fluidically tunable, dual-band patch antenna. (a) Top view. (b) Side view.

II. Principles of Operation and Design Procedure

Fig. 1 shows the topology of the proposed antenna. Two 2.0-mm-diameter channels, filled with mineral oil ($\epsilon_r \approx 2.15$), are located under the nonradiating edges of the patch. In each channel, a metallic cylinder with a length of 32 mm is located that can be moved when the liquid within the channels move. The metal cylinders move along the y-axis from right to left [Fig. 1(a)]. The channels are connected to the inlet and outlet using a symmetric pressure distribution network that ensures the movement of the cylinders within each channel is synchronized (see [8]). The patch operates at around 2.5 GHz without any metal cylinders underneath it. As soon as the cylinders come close to the patch, i.e., when $y_{\text{offset}} \approx 0.0$ mm, the main resonance of the patch splits into two resonances, and the separation increases with increasing y_{offset}.

To understand the dual-band behavior of the antenna, a simple model of the antenna was developed and analyzed. The patch antenna was divided into three segments as shown in Fig. 1(a) with dimensions of 2×32.11 mm^2 for segments 1 and 3, and dimensions of 37.4×32.11 mm^2 for segment 2. The impedances, Z_1, Z_2, and Z_3, at the left radiating edge are determined, and the total input impedance of the antenna is then calculated. In Figs. 1(b) and 2, a detailed breakdown for segment 1 (or 3) is shown. The left portion of the cylinder from the $y = 0$ marker is modeled as an open-ended transmission

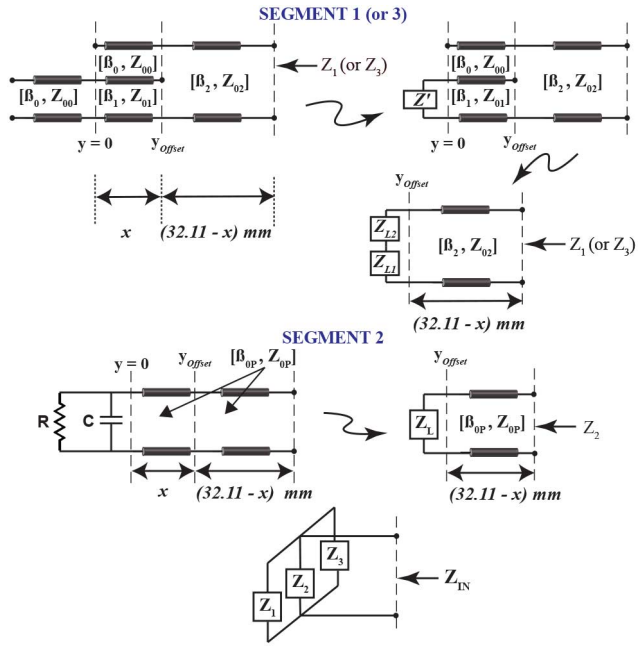

Fig. 2. Transmission-line-based equivalent circuit model of the proposed antenna.

line with wave propagation constant of β_0 and characteristic impedance of Z_{00}. The area between the cylinder and the ground plane, between $y = 0$ and y_{offset}, is modeled as another piece of transmission line with β_1 and Z_{01} terminated at a load of Z'. The area between the cylinder and the patch antenna, between $y = 0$ and y_{offset}, is modeled as another open-ended transmission line with the similar wave propagation constant and characteristic impedance of Z'. The right section from the y_{offset} marker is modeled as a transmission line with β_2 and Z_{02} with the series combination of Z_{L1} and Z_{L2} as its load. The relative dielectric constant for segments 1 and 2 are extracted using CST Microwave Studio and Agilent ADS to compute wave propagation constant (β) values. The characteristic impedances of these transmission line segments are calculated using formulas available in literature to compute characteristic impedance of a microstrip line. The impedance of segment 2 in Fig. 1(a) is calculated using formulas (for transmission line model of patch antenna) available in [9]. The total impedance, Z_{IN}, looking from the left radiating edge is the parallel combination of impedances Z_1, Z_2 and Z_3 (see Fig. 2).

Fig. 3(a) shows the variation of the first and and second resonant frequencies of the antenna as a function of the offset distance, y_{offset}, from both full-wave simulations and the proposed analytical model. As can be observed, as y_{offset} increases, the frequency of the first (second) resonance, f_1 (f_2) decreases (increases) first. Subsequently, as y_{offset} increases further, this trend is reversed. From the simulations (circuit model), the ratio of the frequencies f_2/f_1 changes from 1.05 (1.02) to 1.31 (1.27) as a function of the offset distance. Fig. 4 shows the electric current distribution on the surface of the antenna at the two resonances. Careful examination of these currents reveals that they will result in similar radiation characteristics (polarization, radiation pattern shape, and the direction of maximum radiation) in the far field. Therefore, this dual-band antenna is expected to provide similar radiation characteristics at both of its bands of operation.

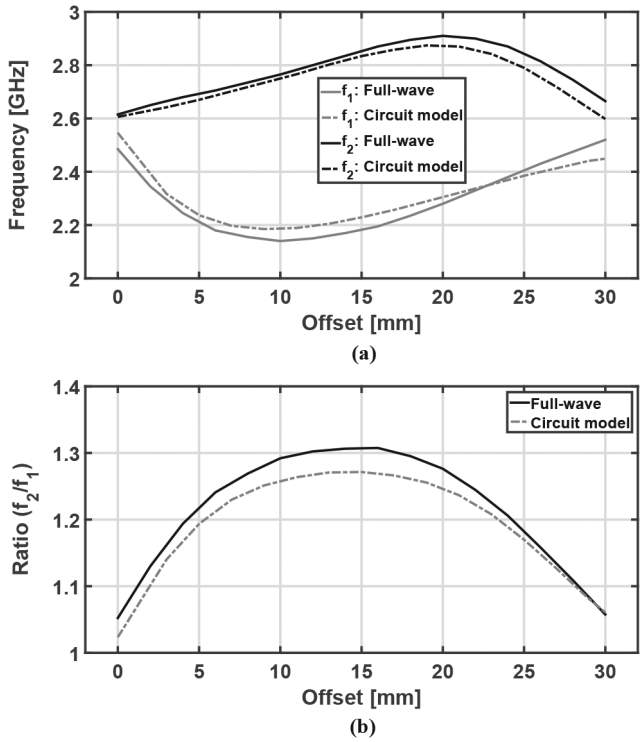

Fig. 3. (a) Variations of the two resonant frequencies. (b) Ratio of the frequencies, f_2/f_1, as a function of y_{offset}.

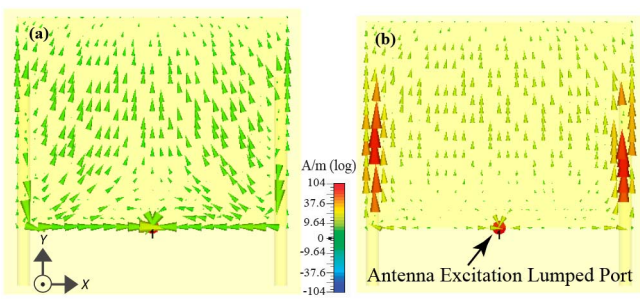

Fig. 4. Simulated electric current distribution on the patch surface for $y_{\text{offset}} = 23$ mm. (a) At $f_1 = 2.355$ GHz. (b) At $f_2 = 2.89$ GHz.

The patch antenna is designed to operate at 2.5 GHz. Accura 60, a type of photopolymer resin that is 3-D printed, is used as the substrate of the antenna. The substrate is 3.35 mm thick and has a dielectric constant of 3.2 and a loss tangent of 0.05 [8], which is included in the simulations. Note that this material was used solely because it was readily available for our use in this proof-of-concept demonstration. However, for a system-level application it is recommended to use 3-D printed materials with lower loss values. The patch antenna has dimensions of 41.4×32.11 mm^2. In the initial simulations, the antenna was fed with a lumped port placed at the edge of the radiating slot [see Fig. 4(b)]. This is done to calculate the input impedance of the antenna at the edge of the radiating slot. The value of this input impedance was subsequently used in the impedance matching process. The response of the antenna was simulated using CST Microwave Studio. The patch and metal cylinders were modeled as copper and brass, respectively, in the simulations. The substrate length is approximately four and a half times of the length of the patch, and the width is twice of the patch width. The length of the substrate was

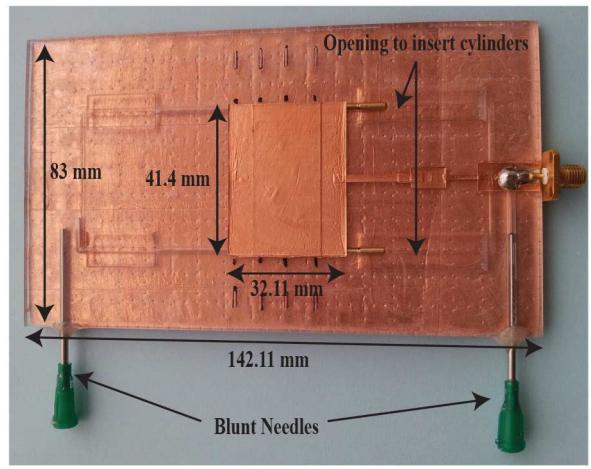

Fig. 5. Photograph of the fabricated prototype with two visible brass cylinders.

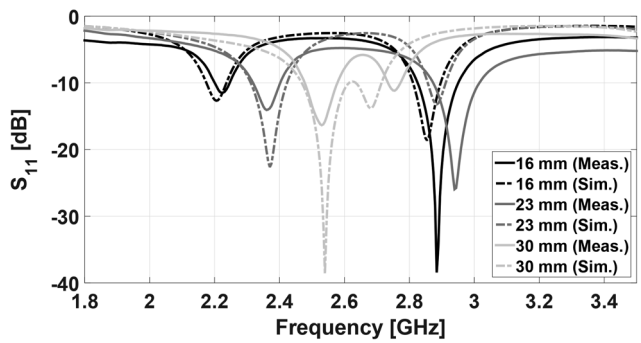

Fig. 6. Simulated and measured input reflection coefficients of the patch antenna for $y_{\text{offset}} = 16$ mm, $y_{\text{offset}} = 23$ mm, and $y_{\text{offset}} = 30$ mm.

chosen to be 4.5 times the patch length so that there was enough space for the metal cylinders to rest without coming in close proximity to the patch and also accommodate the inlet/outlet channels.

III. Prototype Fabrication and Measurement Results

The substrate of the proposed antenna was fabricated using a Dimension Elite 3-D printer and is shown in Fig. 5 (notice that the substrate is transparent). An impedance-matching network consisting of a series of transmission lines was designed to ensure proper matching for all values of y_{offset}. The patch antenna along with the matching network was assembled on top of the substrate with copper tape (see Fig. 5). Two 32-mm-long brass cylinders with diameter 2.0 mm were inserted into the channels. The openings were later covered with 3-D printed pieces and sealed off with epoxy. The channels were filled with mineral oil using a 10-mL syringe through one of the inlets/outlets. After the channels were filled up, the other inlet/outlet was mounted with a partially oil-filled 10-mL syringe. One of the syringes was pressed to move the cylinders together along the channels and position them at a specific y_{offset}. The S_{11} of the antenna was then measured using an Agilent N5225A PNA for three different offsets, $y_{\text{offset}} = 16$ mm, $y_{\text{offset}} = 23$ mm, and $y_{\text{offset}} = 30$ mm. The results are shown in Fig. 6. It can be seen from the results that there are discrepancies between measurements and simulations in the form of frequency shift and lower/higher reflection coefficient values at the resonant frequencies. These can be attributed to several factors such as

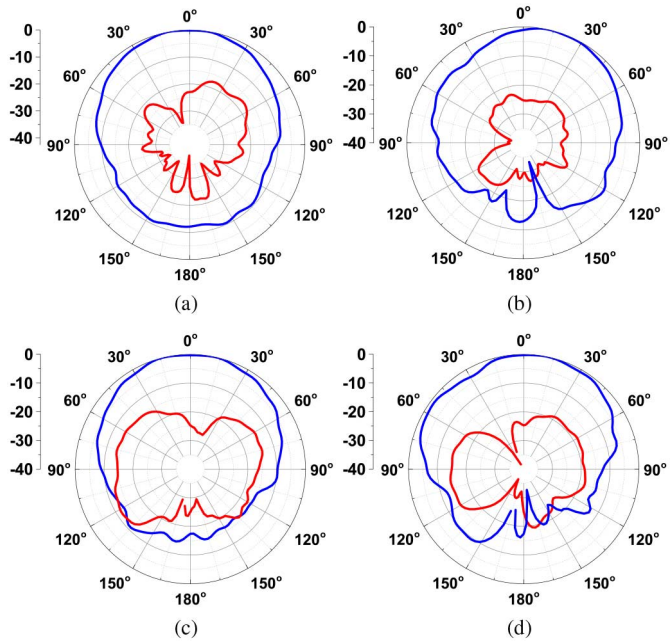

Fig. 7. Measured normalized gain patterns of the antenna. (a)–(d) Radiation patterns [co-pol (blue) and cross-pol (red)] at 2.35 and 2.93 GHz when $y_{\text{offset}} = 23$ mm. (a) H-plane at 2.35 GHz (Max. Gain = 1.48 dBi). (b) E-plane at 2.35 GHz (Max. Gain = 2.31 dBi). (c) H-plane at 2.93 GHz (Max. Gain = 0.45 dBi). (d) E-plane at 2.93 GHz (Max. Gain = 0.41 dBi).

TABLE I
TOTAL EFFICIENCY AND PEAK DIRECTIVITY OF THE ANTENNA AT THE RESONANT FREQUENCIES FOR $y_{\text{offset}} = 16, 23$, AND 30 mm

	Simulation		Measurement	
Frequency [GHz]	2.2	2.85	2.22	2.88
Total Efficiency	28%	29%	27%	31%
Peak Directivity (dBi)	6.38	6.89	6.97	6.36
Frequency [GHz]	2.365	2.88	2.35	2.93
Total Efficiency	33%	22%	32%	25%
Peak Directivity (dBi)	7.15	6.69	7.27	6.49
Frequency [GHz]	2.535	2.675	2.53	2.74
Total Efficiency	34%	21%	38%	18%
Peak Directivity (dBi)	7.34	6.3	7.11	8.11

imperfections arising in the dimensions of the patch antenna and/or matching network due to the use of copper tape and limited accuracy of measurement technique used to characterize dielectric constant and loss tangent values of Accura 60 substrate (see [10]).

The radiation patterns of the antenna were measured using a multiprobe near-field antenna measurement system (Satimo StarLab). Measurements were done for $y_{\text{offset}} = 16$, 23, and 30 mm, respectively. Fig. 7 shows the co- and cross-pol radiation patterns when y_{offset} was 23 mm. The tilt observed in the E-plane pattern is attributed to the presence of the cylinders, the feed network, and relatively long feeding cables along the E-plane. Table I compares the simulated and measured total efficiencies as well as the peak directivity of the antenna for three y_{offset} values. The relatively small total efficiencies are primarily attributed to the high losses of the 3-D printed dielectric substrate. This, however, is not an inherent limitation of the proposed design. The radiation efficiency of the antenna can be significantly enhanced if lower-loss materials are used to implement the substrate. The mechanical tuning speed of the structure is constrained by the 10-mL syringes, the inside surface roughness of the channels, and them being free of any residues that remain from the fabrication process. Based on the availability of various commercial micropumps, the tuning speed of antennas of this type is expected to vary between hundreds of microseconds to hundreds of milliseconds.

IV. CONCLUSION

The design and principles of operation of a new type of dual-band patch antenna with closely spaced bands of operation were presented and discussed. It was also demonstrated that the response of this antenna can be made tunable using a fluidic tuning technique. A simple transmission-line-based equivalent circuit model was also developed to predict the behavior of the two resonances of the antenna when it is tuned using the proposed fluidically tuning mechanism. The frequency variation trend predicted by the model closely matches the trend extracted from the full-wave simulations. A prototype was also fabricated and characterized. Measurement results show a return loss better than 10 dB and consistent, similar radiation patterns at both bands of operation across its entire frequency band of operation. In the specific example discussed in this letter, a frequency ratio of $f_2/f_1 = 1.08$–1.30 was achieved from measurement. The radiation efficiency of this antenna can be enhanced dramatically if a lower-loss dielectric substrate is used. This antenna is expected to be useful both in its static mode of operation (i.e., nontunable) in conventional dual-band systems and its tunable version in systems that need to transmit signals with high (tens of watts) peak power while maintaining linearity.

REFERENCES

[1] N. Haider, D. Caratelli, and A. G. Yarovoy, "Recent developments in reconfigurable and multiband antenna technology," *Int. J. Antennas Propag.*, vol. 2013, pp. 1–14, Jan. 2013.
[2] J. T. Bernhard, *Reconfigurable Antennas*. San Francisco, CA, USA: Morgan and Claypool, 2007.
[3] C. G. Christodoulou, Y. Tawk, S. A. Lane, and S. R. Erwin, "Reconfigurable antennas for wireless and space applications," *Proc. IEEE*, vol. 100, no. 7, pp. 2250–2261, Jul. 2012.
[4] F. Yang and Y. Rahmat-Samii, "A reconfigurable patch antenna using switchable slots for circular polarization diversity," *IEEE Microw. Wireless Compon. Lett.*, vol. 12, no. 3, pp. 96–98, Mar. 2002.
[5] C. W. Jung, M. J. Lee, G. P. Li, and F. D. Flaviis, "Reconfigurable scan-beam single-arm spiral antenna integrated with RF-MEMS switches," *IEEE Trans. Antennas Propag.*, vol. 54, no. 2, pp. 455–463, Feb. 2006.
[6] N. Behdad and M. K. Sarabandi, "Dual-band reconfigurable antenna with a very wide tunability range," *IEEE Trans. Antennas Propag.*, vol. 54, no. 2, pp. 409–416, Feb. 2006.
[7] M. Li and N. Behdad, "Fluidically tunable frequency selective/phase shifting surfaces for high-power microwave applications," *IEEE Trans. Antennas Propag.*, vol. 60, no. 6, pp. 2748–2759, Jun. 2012.
[8] T. Bhattacharjee, H. Jiang, and N. Behdad, "Large-scale fluidic tuning of sub-wavelength periodic structures," *IEEE Antennas Wireless Propag. Lett.*, vol. 14, pp. 190–193, 2015.
[9] C. A. Balanis, "Microstrip antennas," in *Antenna Theory Analysis and Design*, 3rd ed. Hoboken, NJ, USA: Wiley-Interscience, 2005, ch. 14, pp. 811–876.
[10] S. Aguilar *et al.*, "Dielectric characterization of PCL-based thermoplastic materials for microwave diagnostic and therapeutic applications," *IEEE Trans. Biomed. Eng.*, vol. 59, no. 3, pp. 627–633, Mar. 2012.